1 **MFN2-dependent recruitment of ATAT1 coordinates mitochondria motility with α-tubulin**

2 **acetylation and is disrupted in CMT2A**

3 A. Kumar[1], D. Larrea[2], M.E. Pero[1,3], P. Infante[4], M. Conenna[4], G.J. Shin[5], W. B. Grueber[5,6],

4 L. Di Marcotullio[4,7], E. Area-Gomez[2,8], and F. Bartolini[1,*]

5

6 [1]Department of Pathology & Cell Biology, Columbia University Irving Medical Center, 10032, New York, NY, USA

7 [2]Department of Neurology, Columbia University Irving Medical Center, 10032, New York, NY, USA

8 [3]Department of Veterinary Medicine and Animal Production, University of Naples Federico II, 80137, Naples, Italy

9 [4]Department of Molecular Medicine, 1st University of Rome "La Sapienza", 00161, Rome, Italy

10 [5]Department of Neuroscience, Zuckerman Mind Brain Behavior Institute, Columbia University, 10027, New York,

11 NY, USA

12 [6]Department of Physiology & Cellular Biophysics, Zuckerman Mind Brain Behavior Institute, Columbia University,

13 10032, New York, NY, USA

14 [7]Istituto Pasteur-Fondazione Cenci Bolognetti, University of Rome La Sapienza, Rome, Italy.

15 [8]Current address: Department de Biología Celular y Molecular, Centro de Investigaciones Biológicas, MARGARITA

16 SALAS, CSIC, 28040, Madrid, Spain

17

18

19 ***Corresponding author:** fb2131@columbia.edu

20

21

22

23

24

25 **Running title:** MFN2 coordinates mitochondria motility and tubulin acetylation

26 **Key Words:** Microtubules, acetylated tubulin, ATAT1, HDAC6, MFN2, CMT2A, mitochondria

27 motility, axon degeneration

28 **Abbreviations:** Microtubule, MT; post-translational modifications, PTMs; Charcot-Marie-Tooth

29 Type 2A, CMT2A; Mitofusin-2, MFN2; α-tubulin acetyl transferase 1, ATAT1; Histone

30 deacetylase 6, HDAC6; outer mitochondrial membrane, OMM; endoplasmic reticulum, ER;

31 Mitofusin-1, MFN1; mitochondria-associated ER membranes, MAMs; trichostatin A, TSA;

32 tubulin tyrosine ligase, TTL

33

Abstract

Acetylated microtubules play key roles in the regulation of mitochondria dynamics. It has however remained unknown if the machinery controlling mitochondria dynamics functionally interacts with the α-tubulin acetylation cycle. Mitofusin-2 (MFN2), a large GTPase residing in the mitochondrial outer membrane and mutated in Charcot-Marie-Tooth type 2 disease (CMT2A), is a regulator of mitochondrial fusion, transport and tethering with the endoplasmic reticulum. The role of MFN2 in regulating mitochondrial transport has however remained elusive. Here we show that mitochondrial contacts with microtubules are sites of α-tubulin acetylation, which occurs through the MFN2-mediated recruitment of α-tubulin acetyltransferase 1 (ATAT1). We discover that this activity is critical for MFN2-dependent regulation of mitochondria transport, and that axonal degeneration caused by CMT2A MFN2 associated mutations, R94W and T105M, may depend on the inability to release ATAT1 at sites of mitochondrial contacts with microtubules. Our findings reveal a function for mitochondria in regulating acetylated α-tubulin and suggest that disruption of the tubulin acetylation cycle play a pathogenic role in the onset of MFN2-dependent CMT2A.
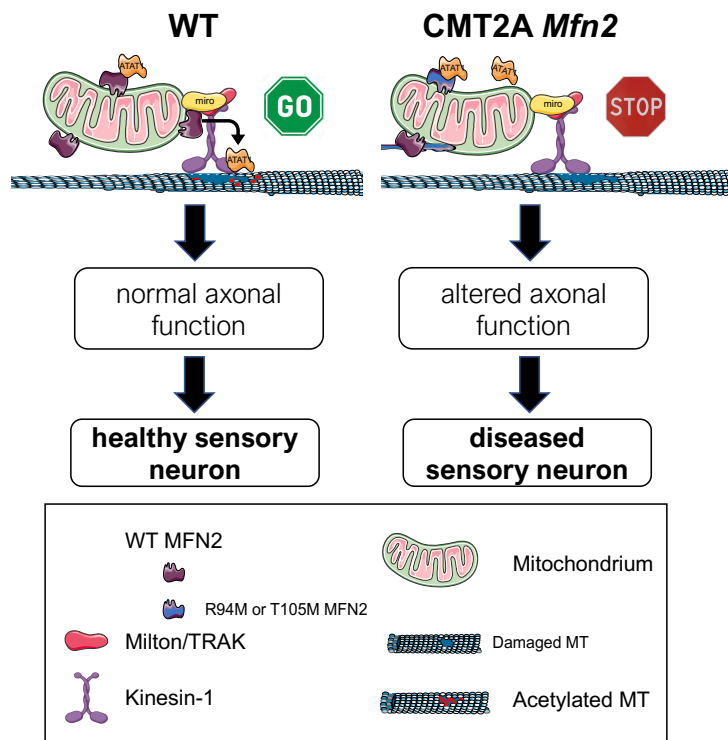
Highlights

- Mitochondria contacts with MTs are hotspots of α-tubulin acetylation through the recruitment of ATAT1 by MFN2
- Mutations in MFN2 associated with CMT2A disease lose this activity by sequestering ATAT1
- Distal axonal degeneration caused by loss of MFN2 depends on acetylated tubulin-mediated mitochondria transport

eTOC Recruitment of ATAT1 to mitochondria by MFN2 is critical for axonal viability through the regulation of mitochondria transport, and is disrupted in CMT2A

Introduction

Microtubules (MTs) are key cytoskeletal elements involved in a multitude of functions in all eukaryotic cells. MTs are polarized polymers (comprised of a plus and minus end) constructed by the regulated polymerization of α- and β-tubulin dimers, and their dynamic nature allows them to switch between growth and shrinkage [1]. In neurons, MTs are critical because they support trafficking while providing segregation of functional sub compartments [2]. In vertebrates, MT plus ends uniformly orient toward the distal end of axons, while MTs are arranged with mixed polarity in dendrites [3]. In addition to ensuring structural support, MTs act as intracellular highways for protein motors of the kinesin and dynein family to deliver cargoes via anterograde or retrograde transport respectively. Directional transport is enabled by the structural polarity of MTs, which is recognized by motor proteins that drive transport to either the minus end (dynein) or plus end (most kinesins) [4]. In addition to structural polarity, tubulin post-translational modifications (PTMs) that accumulate on stable MTs are crucial modulators of neuronal transport and their dysregulation has been recently associated with the pathogenesis of both neurodevelopmental and neurodegenerative diseases [5, 6].

Acetylated MTs are a subset of stable MTs with key roles in the regulation of axonal transport and mitochondrial dynamics: along with providing preferential tracks for kinesin-1- and dynein-dependent mitochondria transport, two properties of acetylated MTs, their stability and flexibility, make them uniquely adapted to sustain mechanical stress caused by surface tension and organelle/organelle interactions [7-9]. It is perhaps thanks to these properties that mitochondria fusion, fission and ER/mitochondria contact occur selectively on acetylated MTs [10, 11].

Acetylation of lys-40 in α-tubulin is predominantly regulated by the tubulin N-acetyltransferase 1 (αTAT1 or ATAT1) and histone deacetylase 6 (HDAC6), two soluble enzymes that catalyze the forward and backward reaction, respectively [12-15]. Tubulin acetylation on lys-40 is an α-tubulin PTM marking the luminal surface of MTs [16 , 17], a unique feature that helps the MT lattice cope with mechanical stress via reduced lateral interactions between protofilaments [7] and presumably by facilitating MT self-repair through incorporation of GTP-bound tubulin subunits [9, 18].

It is thought that in neurons a large pool of ATAT1 is recruited to the MT lattice by vesicle "hitchhiking" prior to entering the lumen at MT ends or at cracks in the MT lattice [19-22]. In migrating cells, clathrin-coated pits control MT acetylation through a direct interaction of the

95   ATAT1 with the clathrin adaptor AP2 [23]. The rules dictating the selection of the docking sites

96   on vesicles, clathrin-coated pits or MTs are however unknown. Similarly unexplored is whether

97   other organelles can act as docking sites for ATAT1 binding. These are important questions to

98   address, as either hypoacetylation or hyperacetylation of tubulin are predicted to negatively affect

99   MT-dependent functions, either by reducing the local flexibility of the MT (thus promoting further

100   breakage upon bending) or by inhibiting MT dynamics while promoting premature tubulin

101   longevity.

102   In sensory neurons acetylated tubulin is an essential component of the mammalian

103   mechanotransduction machinery through its regulation of cellular stiffness and TRP channel

104   activity [24-26], and loss of acetylated tubulin was reported as a neuropathological feature of

105   vincristine-induced toxicity [27]. Indeed, enhancing tubulin acetylation by HDAC6 inhibitors has

106   been largely successful in restoring axonal integrity and myelination of toxic and genetically

107   inherited forms of peripheral neuropathy, prompting multiple companies to develop and test

108   HDAC6 inhibitors in models of peripheral neuropathies including Charcot-Marie-Tooth disease

109   (CMT) [27-29]. Given the multitude of HDAC6 substrates in addition to tubulins, however, the

110   mechanisms underlying this rescue remain unclear.

111   Charcot-Marie-Tooth type 2A (CMT2A) disease is a predominantly axonal form of familial

112   peripheral neuropathy causing sensory loss that results from degeneration of long peripheral axons

113   [30]. Inherited dominant mutations in the mitochondrial fusion protein mitofusin-2 (MFN2), a

114   large GTPase residing in the outer mitochondrial membrane (OMM) and endoplasmic reticulum

115   (ER), are the most common causes of CMT2A, and the majority of MFN2 mutations affect the

116   amino terminal GTPase domain, with disease onset in the first two years of life and an aggressive

117   clinical course [31, 32]. Like acetylated tubulin, MFN2 plays crucial roles in mitochondria

118   dynamics, including regulation of fusion, motility, and ER/mitochondria contacts [33]. Defects in

119   mitochondria dynamics are typically associated with CMT pathogenesis, including CMT caused

120   by mutant MFN2 [34-37]. However, the mechanism by which mutant MFN2 contributes to

121   CMT2A remains elusive.

122   Together with mitofusin-1 (MFN1), MFN2 regulates mitochondrial fusion, which is essential

123   to maintain proper mitochondrial distribution, shape and degradation [33]. In addition, MFN2

124   plays a critical role in ER-mitochondrial tethering, which is independent of its fusion function, by

125   bonding mitochondria with mitochondria-associated ER membranes (MAMs) to allow for ATP,

126 Ca^{2+} and lipid transfer [34, 38-41]. Accordingly, MFN2 also regulates the rate of cholesterol

127 esterification, which was proposed to be a proxy of MAM function, and the extent of contact points

128 between the ER and mitochondria [42].

129 A fusion-independent role for MFN2 in regulating mitochondrial axonal transport has been

130 reported. Loss of MFN2 or MFN2 disease mutants selectively alter mitochondrial axonal motility

131 and distribution [35, 43, 44]. In addition, MFN2 deficiency in human spinal motor neurons

132 interferes with mitochondrial transport while reducing both mRNA and protein levels of kinesin

133 and dynein motors [45], which may further contribute to impaired mitochondrial motility.

134 Furthermore, both MFN1 and MFN2 interact with mammalian miro (miro1/miro2) and

135 milton/TRAK (OIP106/GRIF1) proteins, members of the molecular machinery that links

136 mitochondria to kinesin motors [43], and overexpression of MFN1 rescues the axonal degeneration

137 caused by MFN2 mutants *in vitro* and *in vivo* [44, 46].

138 Altogether, these data support the notion that MFN2 may directly influence mitochondrial

139 positioning, and that loss of this function contributes to the degeneration of long axons, which are

140 particularly sensitive to failures in meeting local energy demands. This model is consistent with

141 the observation that most of the genes mutated in predominantly axonal forms of CMT have roles

142 in mitochondrial motility, suggesting that impaired mitochondrial transport may be a common

143 mechanism of pathogenesis shared by seemingly unrelated proteins associated with an increased

144 risk for CMT [36]. Despite this compelling evidence, the molecular basis underlying MFN2-

145 dependent regulation of mitochondria positioning remains poorly understood. Furthermore, while

146 loss of MFN2 induces axonal neuropathy, the detailed mechanisms by which MFN2 deficiency

147 results in axonal degeneration are unestablished.

148 In this study, we find that mitochondria contacts with MTs are hotspots of tubulin acetylation

149 through the recruitment of ATAT1 by MFN2 onto mitochondrial outer membranes and that this

150 activity is affected by MFN2 R94W and T105M CMT2A mutations. Furthermore, we provide

151 evidence that axonal degeneration caused by MFN2 loss of function in DRG neurons depends on

152 loss of acetylated tubulin by disrupting mitochondria motility rather than mitochondrial fusion or

153 tethering with the ER.

154

155

156

157   **Results**

158   *MFN2 is a novel regulator of tubulin acetylation*

159   Despite the intimate relationship between acetylated MTs and mitochondria dynamics, it

160   has remained unknown if the machinery controlling mitochondria motility and/or hetero-

161   homotypic mitochondrial contacts functionally interacts with the α-tubulin acetylation cycle. To

162   test this hypothesis, we measured levels of acetylated α-tubulin in immortalized Mfn2 KO mouse

163   embryonic fibroblast (MEF) cells with reported defects in mitochondria dynamics and functional

164   tethering with the ER [47]. By immunoblot and immunofluorescence analyses, we found that while

165   de-tyrosinated tubulin levels were unaffected, loss of MFN2 reduced acetylated tubulin by more

166   than 50% compared to WT controls (Fig. 1A-E and Fig. S1A-D). Loss of acetylated tubulin in

167   these cells also correlated with a decrease in the abundance of GTP-tubulin islands, the putative

168   entry sites for the tubulin acetyltransferase ATAT1 into the MT lumen and hotspots of MT self-

169   repair by incorporation of GTP-bound tubulin subunits [48-51] (Fig. 1F,G).

170   We measured MT plus end dynamics by following the behavior of individual MTs in WT

171   and Mfn2 KO cells transfected with GFP-tubulin and found that lack of MFN2 expression almost

172   doubled MT dynamicity, an effect due to an increase in MT growth and shrinkage rates (Table 1).

173   The rise in MT dynamicity correlated with a significant loss of MT stability. To test this, we

174   measured the amount of residual MT polymer resisting depolymerization that was induced by mild

175   detergent extraction prior to fixation and immunofluorescence staining (Fig. 1H,I). Importantly,

176   both acetylated tubulin levels and MT dynamics were normalized in Mfn2 KO cells by the HDAC6

177   inhibitor trichostatin A (TSA) (Fig. S1A-D and Table S1), suggesting that the increase in MT

178   dynamicity resulted from loss of α-tubulin acetylation in cells deprived of MFN2.

179

Figure 1
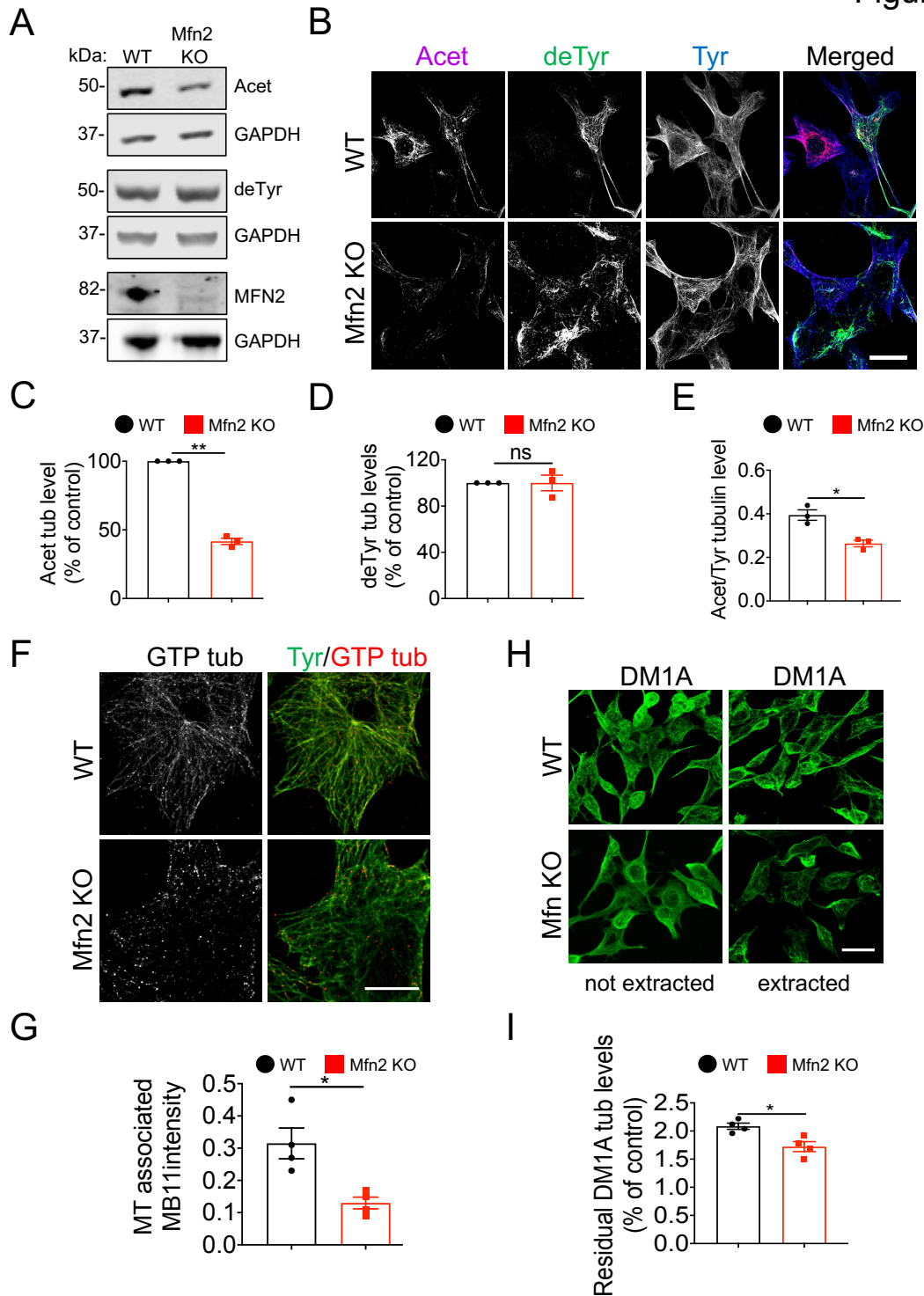
Figure 1. **MNF2 regulates α-tubulin acetylation, MT dynamics and MT stability in MEFs.** (A) Representative immunoblot of WT and Mfn2 KO whole MEF lysates. Acet, acetylated tubulin; deTyr, detyrosinated tubulin; Mfn2, mitofusin 2; GAPDH, loading control. (B) Representative immunofluorescence images (max projections from z-stacks) of WT and Mfn2 KO MEFs. Tyr, tyrosinated tubulin; Acet, acetylated

184   tubulin; Tyr, tyrosinated tubulin. (C) Quantification of acetylated (Acet) and (D) detyrosinated (deTyr) tubulin

185   signal normalized to WT control levels (n=150-175 cells). (E) Quantification of acetylated (Acet) to tyrosinated

186   (Tyr) tubulin immunofluorescence signal intensity ratio in WT and Mfn2 KO MEFs. (F) GTP tubulin staining

187   in WT and Mfn2 KO MEFs using hMB11 antibody staining. (G) Quantification of GTP-tubulin (MB11)

188   immunofluorescence signal intensity associated with MTs in WT and Mfn2 KO MEFs (n=20-25 cells). (H)

189   Representative immunofluorescence images of residual MT staining (DM1A) in WT and Mfn2 KO extracted

190   MEFs. (I) Quantification of residual DM1A tubulin levels in WT and Mfn2 KO MEFs treated as in H (n=100-

191   125 cells). Data are expressed as median with interquartile range. n= 3 independent experiments * p<0.05; **

192   p<0.01; ns non-significant by Mann–Whitney U test. Scale bars, 10 µm.

	WT	**Mfn2 KO**
Growth rate (µm/s)	0.05 ± 0.02	0.13 ± 0.006 *
Shrinkage rate (µm/s)	0.07 ± 0.004	0.12 ± 0.01 *
Catastrophe freq. (s-1)	0.06 ± 0.006	0.06 ± 0.004
Rescue freq. (s-1)	0.08 ± 0.006	0.08 ± 0.006
% Growth	35.5 ± 1.92	44.15 ± 0.95 ***
% Shrinkage	34.05 ± 0.87	36.48 ± 1.27 *
% Pause	29.58 ± 0.62	20.1 ± 1.45
MT lifetime (s)	58.25 ± 2.14	60.5 ± 1.73
MT dynamicity (µm/min)	5.96 ± 0.42	10.43 ± 0.25 ***
Number of MTs	20	20

Table 1. MFN2 regulates MT dynamics in MEFs. MT dynamics were measured from time-lapse analysis of GFP-tubulin-labeled MTs using epifluorescence microscopy (1f/5s). Parameters characterizing MT dynamics, such as the growth rate, the shrinkage rate, the frequency of 'catastrophe' (transitions from growth/pause to shortening) and 'rescue' (transitions from shortening to growth/pause) events, as well as the average amount of time spent by MTs in growth, shrinkage and pausing, MT lifetime and MT dynamicity (#of growth + shrinkage events/lifetime). Data are mean ± SEM from 3 independent experiments. * p<0.05; *** p<0.001 by Student's t-test.

193

194

195

Tubulin acetylation is required for MFN2-dependent regulation of mitochondrial motility but not for mitochondrial fusion or functional tethering to the ER

We observed that the co-localization of mitochondria with MTs was reduced in Mfn2 KO cells but was restored when Mfn2 KO cells were treated with TSA (Fig. S1E,F). Hence, we determined whether increasing acetylated tubulin levels by TSA also reestablished regular mitochondria dynamics, and/or mitochondrial associated ER-membrane (MAM) function, mitochondrial features affected by loss of MFN2 expression (Fig. 2). We observed that TSA normalized both central and peripheral mitochondrial displacement velocity as well as mitochondria distribution and contacts with MTs in Mfn2 KO cells (Fig. 2A-C and Fig. S1E,F). However, while mitochondria elongated morphology was partially reestablished in Mfn2 KO cells treated with TSA, increasing acetylated tubulin completely failed to recover mitochondria fusion, an activity significantly compromised in cells deprived of MFN2 (Fig. 2D,E). Identical results were obtained using tubacin, a more potent and highly selective HDAC6 inhibitor (Fig. 2F-I) [52].

We inquired whether the rescue of mitochondrial dynamics was dependent on acetylated tubulin or a general gain in MT stability resulting from tubulin acetylation. To test this, we adopted Iqgap1 KO MEFs, a cell line with normal MFN2 levels but naturally deprived of detyrosinated and acetylated MTs, two independent subsets of stable MTs [53] (Fig. S2). By analogy with Mfn2 KO cells, we found that loss of IQGAP1 also resulted in defective MT and mitochondrial dynamics (Fig. S3 and Table S2), consistent with a role for modified MTs in regulating mitochondria homeostasis. However, increasing detyrosinated tubulin by tubulin tyrosine ligase (TTL) silencing did not normalize mitochondrial dynamics to the extent of TSA treatment (Fig. S3E-I), suggesting that rescue of mitochondria dynamics was dependent on the selective increase in acetylated tubulin rather than a general gain in MT stability (Fig. S2,3 and Table S2).

Next, we tested the effects of restoring acetylated tubulin levels on loss of MAM function by analyzing the synthesis and transfer of phospholipid between ER and mitochondria, a known proxy of MAM activity, as well as changes in lipid classes by lipidomics analysis in Mfn2 KO cells [34, 54]. MAM is a transient specialized subdomain of the ER with the characteristics of a lipid raft. The temporary formation of MAM domains in the ER regulates several metabolic pathways, including lipid and Ca^{2+} homeostasis and mitochondrial activity [38, 55]. Alterations in the formation of MAM domains have been reported to induce significant changes in lipid metabolism in several pathologies including neurodegenerative disease [39, 55]. In particular,

227 defects in MAM activity have significant detrimental effects on the regulation of cholesterol and

228 its esterification into cholesteryl esters [56]. Equally important, defects in MAM impair the

229 regulation of sphingomyelin (SM) turnover and its hydrolysis into ceramide species [57, 58].

230   We found that Mfn2KO cells display significant increases in sphingomyelin and

231 cholesterol with concomitant decreases in cholesteryl esters and ceramide levels (Fig. 2J,K) and

232 that these changes could be rescued by HDAC6 inhibition (Fig. 2J,K). However, TSA failed to

233 normalize MAM-dependent phospholipid synthesis measured by incorporation of radiolabeled ^{3}H-

234 Ser into newly synthesized ^{3}H-PtdSer (PS) and (H) ^{3}H-PtdEtn (PE) (Fig. 2L).

235   Altogether, our results demonstrate a previously unrecognized role for MFN2 in the

236 regulation of α-tubulin acetylation and suggest that this activity is important for MFN2-dependent

237 control of mitochondria motility and lipid-raft MAM composition, but not for MFN2-dependent

238 mitochondrial fusion or functional mitochondrial/ER tethering. Furthermore, our results in Iqgap1

239 KO cells support the notion that acetylated tubulin is a modulator of mitochondria dynamics *per*

240 *se* and suggest that the machinery controlling mitochondria motility may regulate the α-tubulin

241 acetylation cycle at sites of mitochondria contacts with MTs.

242

243

244

245

246

247

248

249

250

251

252

253

254

Figure 2
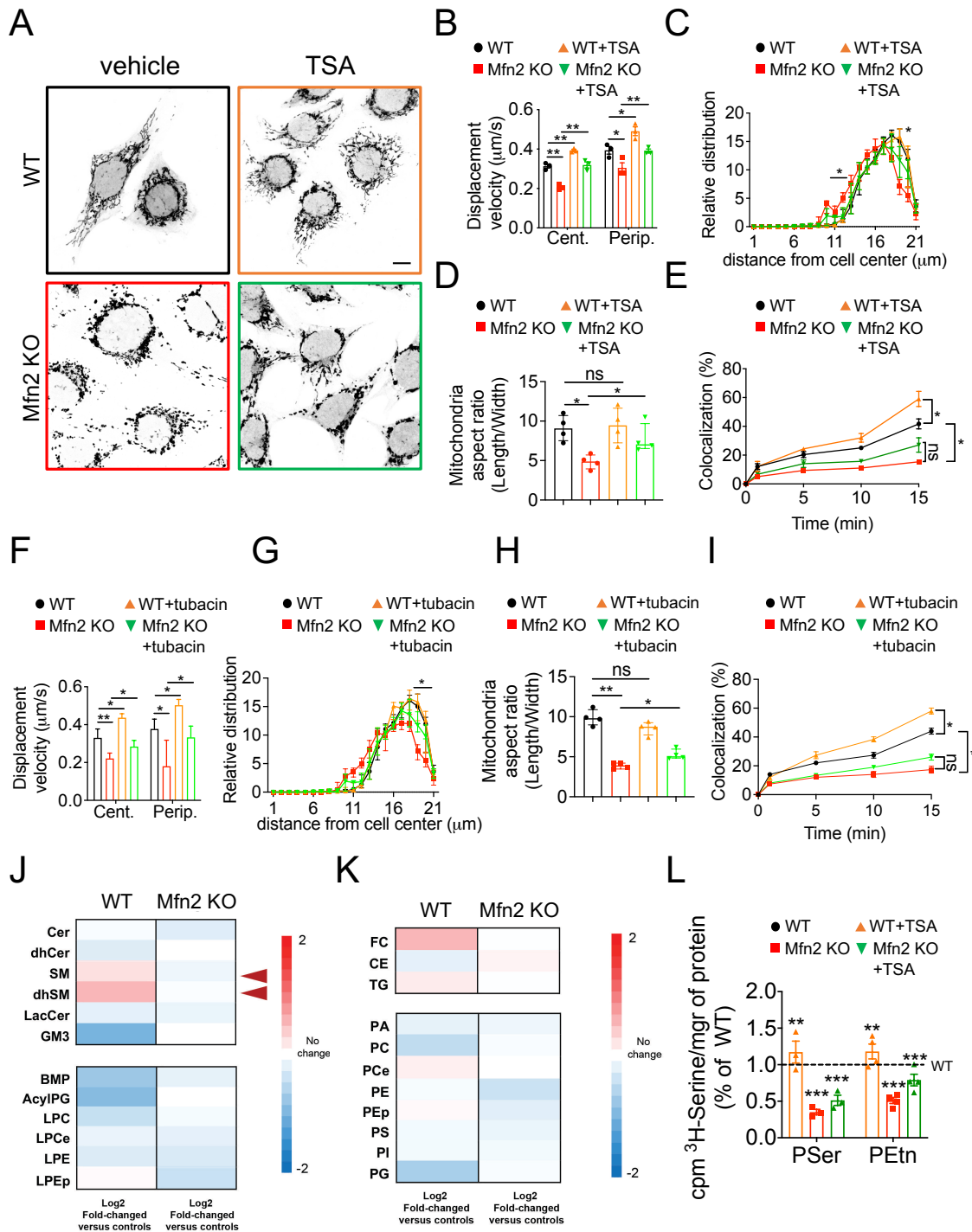
Figure 2. Restoring acetylated tubulin in Mfn2 KO MEFs rescues mitochondria motility and cholesterol esterification but not mitochondria fusion or phospholipid synthesis defects. (A) WT and Mfn2 KO cells were stained with mitoTracker Red and treated with TSA (10 µM) or vehicle control for 6 h. Scale bar, 10 µm. (B) Quantification of mitochondrial displacement velocity analyzed from movies acquired for 3 min (1f/2s) in

11

259   cells treated as in A. Movies were analyzed using Image J manual tracking plug-in. (C) Quantification of relative

260   distribution of mitochondria (#) to the geometrical cell center in cells treated as in A (D) Quantification of

261   mitochondria aspect ratio (length/width) in cells treated as in A (n = 100-120 mitochondria from 4 independent

262   experiments). (E) Quantification of mitochondria fusion using mitoDendra expression in cells treated as in A.

263   (F) Quantification of mitochondrial displacement velocity analyzed from movies acquired for 3 min (1f/2s) in

264   cells treated with tubacin (20 µM). Movies were analyzed using Image J manual tracking plug-in (125-150

265   mitochondria/10-12 cells from 3 independent experiments). (G) Quantification of relative distribution of

266   mitochondria (#) to the geometrical cell center in cells treated with tubacin (20 µM). (H) Quantification of

267   mitochondria aspect ratio (length/width) in cells treated with tubacin (20 µM). (I) Quantification of mitochondria

268   fusion using mitoDendra expression in cells treated with tubacin or control vehicle for 6 h. (G,H and I) n= 125-

269   150 mitochondria from 3-4 independent experiments. (J,K) Heatmap representation of changes in lipid classes

270   in MFN2 KO MEFs treated with vehicle control or TSA (10 nM). (L) Phospholipid synthesis and transfer

271   between ER and mitochondria in WT and Mfn2 KO MEFs treated with vehicle control or TSA (10 nM) for 6 h.

272   Incorporation of ^{3}H-Ser into ^{3}H-PtdSer (PS) and (H) ^{3}H-PtdEtn (PE) after 2 h and 4 h expressed as % of the

273   average value measured in the controls. Cer: ceramide, dhcer: dihydroceramide, SM: sphingomyelin, dhSM:

274   dehydrosphingomyelin, GM3: monosialodihexosylganglioside. BMP: Bis(monoacylglycerol)phosphate ,Acyl-

275   PG, acylated phosphatidylglycerol, LPC: Lysophosphatidylcholine, LPCe: Lysophosphatidylcholine

276   plasmalogen, LPE: Lysophosphatidylethanolamine, LPEp: Lysophosphatidylethanolamine plasmalogen; FC:

277   free cholesterol, CE: cholesteryl esters; PA: phosphatidic acid; PC: Phosphatidylcholine; PCe

278   Phosphatidylcholine plasmalogen; PE: Phosphatidylethanolamine; PEp: Phosphatidylethanolamine

279   plasmalogen; PS: Phosphatidylserine; PI: Phosphatidylinositol; PG: Phosphatidylglycerol. * p<0.05; ** p<0.01;

280   *** p<0.001; ns non-significant by Kruskal-Wallis test. Data are expressed as median with interquartile range.

281

282   ***MFN2 regulates α-tubulin acetylation by recruiting ATAT1 at sites of mitochondrial contacts***

283   ***with MTs***

284   We began to investigate the mechanisms underlying MFN2 regulation of acetylated α-

285   tubulin by measuring levels and localization of ATAT1 and HDAC6 in Mfn2 KO cells. HDAC6

286   expression was three-fold higher in these cells, in contrast to ATAT1 levels, which remained

287   unaffected (Fig. S4A,B). Loss of MFN2 expression did not affect the percentage of cells in mitosis

288   either (Fig. S4C,D). However, when intracellular membranes were subjected to crude fractionation

289   to isolate the cytosolic from the nuclear and ER fractions, unlike HDAC6 which remained mostly

290   cytosolic, ATAT1 appeared in the cytosolic and in the nuclear/ER portion in WT cells but re-

291   distributed more prominently to the nuclear/ER fraction in Mfn2 KO cells (Fig. S4E-G).

292   Accordingly, co-localization of endogenous ATAT1 with the ER appeared to be increased in Mfn2

293   KO cells compared to WT cells (Fig. S4H-J).

294   We hypothesized that MFN2 may negatively regulate ATAT1 association with the ER by

295   localizing ATAT1 to mitochondria outer membranes, and that this localization may facilitate the

296   access of ATAT1 to openings of the MT lattice at sites of mitochondria contacts with MTs. High

297   resolution confocal microscopy of endogenous proteins revealed punctuate localization of ATAT1

298   to mitochondria membranes or MFN2, and this co-localization was lost in cells deprived of MFN2

299   expression (Fig. 3A-F). Localization of ATAT1 to mitochondria was likely to be dependent on the

300   association of MFN2 with an ATAT1 N-terminal fragment (1-242) inclusive of its catalytic

301   domain, as demonstrated by the *in situ* validation of this interaction using the proximity ligation

302   assay (Fig. 3G,H) and conventional pull down analyses from whole cell lysates using full length

303   or C-terminally truncated versions of ATAT1 (Fig. 3I-K).

304   Altogether, our data demonstrate that ATAT1 associates with mitochondria and that this

305   localization is dependent on the binding of the catalytic domain of ATAT1 with MFN2.

306

307

308

309

310

311

312

313

314

315

316

317

318

319

320

321

322

323
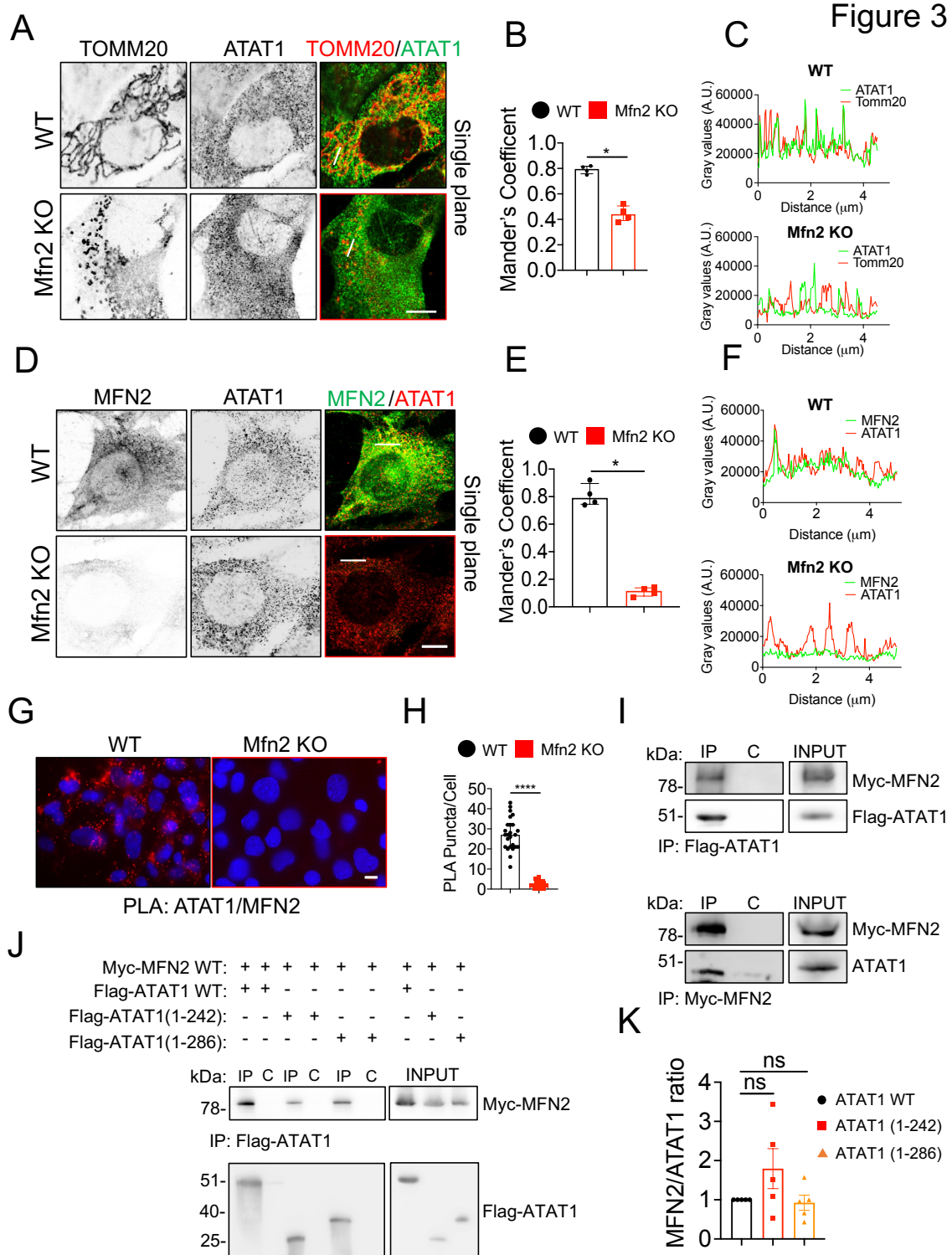
Figure 3. MFN2 localizes the ATAT1 to mitochondria outer membranes in MEFs. (A) Airyscan confocal analysis of mitochondria (TOMM20) and ATAT1 in WT and Mfn2 KO MEFs. Scale bar, 5 µm. (B) Quantification of localization of ATAT1 at mitochondria as in (A) by Mander's correlation coefficient. (C) Line

327   scan analysis of mitochondria and ATAT1 localization from selected regions in (A). Lines are shown as white

328   bars in (A). (D) Airyscan confocal analysis of ATAT1 and MFN2 localization in WT and Mfn2 KO MEFs. Scale

329   bar, 5 μm. (E) Quantification of localization of ATAT1 and MFN2 as in (D) by Mander's correlation coefficient.

330   (F) Line scan analysis of MFN2 and ATAT1 localization from selected regions in (D). Lines are shown as white

331   bars in (D). (G) Immunofluorescence analysis of MFN2 and ATAT1 PLA signal in WT and Mfn2 KO MEFs.

332   Scale bar, 10 μm. (H) Quantification of PLA puncta per cell in WT and Mfn2 KO MEFs. n= 50-55 cells from 3

333   independent experiments. (I) Interaction between ATAT1 and MFN2 was detected by immunoprecipitation (IP)

334   followed by immunoblot analysis with the indicated antibodies (upper panel). Similarly, interaction between

335   endogenous ATAT1 and transfected Myc-MFN2 WT was detected in HEK293T cells (lower panel). (J)

336   HEK293T cells were co-transfected with Myc-MFN2 WT and Flag-ATAT1 WT or Flag-ATAT1 (1-242) or

337   Flag-ATAT1 (1-286). Interaction between MFN2 and ATAT1 WT or mutants was detected by co-

338   immunoprecipitation followed by immunoblot analysis with the indicated antibodies. (K) Normalized MFN2 to

339   ATAT1 signal ratio from (J) was plotted. Data are expressed as median with interquartile range. n = 35-50 cells

340   from 3-4 independent experiments. * $p<0.05$; **** $p<0.001$; ns non-significant by Mann–Whitney U test (3B,E

341   and H) and Kruskal-Wallis test (3K).

342

Loss of acetylated tubulin may underlie CMT2A disease

344   Most MFN2 CMT mutations are missense, and all produce a dominant inheritance pattern,

345   suggesting that mutations in MFN2 lead to either a gain of function or haploinsufficiency [59, 60].

346   Furthermore, recent work supports the notion that restoring MNF1:MFN2 balance by increasing

347   levels of its homologous protein MFN1 is a potential therapeutic approach for CMT2A [46]. The

348   reason for this compensation is unclear, although both MFN2 and MFN1 have been implicated in

349   mitochondria fusion. To determine the involvement of MFN2-dependent regulation of tubulin

350   acetylation in CMT2A disease we investigated whether: 1) mutations in MFN2 affect the

351   interaction with ATAT1 and/or fail to restore normal acetylated tubulin levels in Mfn2 KO cells;

352   2) MFN1 compensates for loss of MFN2 by restoring tubulin acetylation in Mfn2 KO cells; 3) loss

353   of acetylated tubulin by MFN2 depletion is conserved in sensory neurons and sufficient to induce

354   axonal fragmentation, a phenotype associated to axonal forms of CMT disease including CMT2A.

355   We found that MFN2 R94W and T105M, two of the most common N-terminal CMT

356   mutations in MFN2 [61-63] bind to ATAT1 with higher affinity than WT MFN2 (Fig. 4A-C). In

357   addition, while immunofluorescence analysis showed significant higher co-localization of

358   endogenous ATAT1 only with the transfected T105M mutant (Fig. 4D,E), both mutations failed

359   to rescue normal acetylated tubulin levels when expressed in Mfn2 KO cells (Fig. 4F,G). This

360   result was in contrast with ectopic expression of MFN1, which was able to compensate for loss of

361   MFN2 on acetylated tubulin levels in Mfn2 KO cells (Fig. 4H,I).

362   A complex between miro/Milton (TRAK) and MFN2 has been previously shown, and miro

363   has been implicated in regulating MFN2-dependent mitochondrial fusion in response to

364   mitochondrial Ca^{2+} concentration [43]. We tested whether also ATAT1 interacted with miro and/or

365   kinesin heavy chain (Kif5c) and determined the potential effects of mutant MFN2 on the formation

366   of these complexes. We found that ectopic ATAT1 co-immunoprecipitated with both endogenous

367   miro2 and kif5c and that ectopic expression of mutant MFN2 R94W or T105M significantly

368   lowered the affinity of these bindings (Fig. 4J-M). Taken together, these data demonstrate that

369   regulation of acetylated tubulin is an activity shared by MFN1 and that loss of acetylated tubulin

370   may play a primary role in CMT2A *via* the sequestering effect of MFN2 mutations on ATAT1

371   binding.

372   These observations became particularly meaningful when we tested the consequences of

373   loss of MFN2 in sensory neurons and the effects of HDAC6 inhibition on these phenotypes. By

374   analogy with Mfn2 KO cells, silencing of MFN2 expression reduced acetylated tubulin levels both

375   in adult mouse DRG neurons grown in culture and in cell bodies of somatosensory neurons of third

376   instar stage *Drosophila* larvae (Fig. 5A-D). Similar to Mfn2 KO MEFs, we observed localization

377   of endogenous ATAT1 and MFN2 in DRG neurons (Fig. S5A-C) and significant reduction in the

378   extent of ATAT1 localization to mitochondrial membranes in neurons silenced for Mfn2

379   expression in both proximal and distal portion of the axon (Fig. S5D-F). Importantly, cultured

380   sensory neurons deprived of MFN2 acquired a dying-back degeneration phenotype starting from

381   distal regions of the axon, as indicated by the appearance of retraction bulbs at the onset of axonal

382   fragmentation (Fig. 5E and F). We observed that loss of acetylated tubulin preceded axonal

383   degeneration in DRG neurons deprived of MFN2 for shorter times (Fig. S5G-J) and that HDAC6

384   inhibition, which significantly rescued normal acetylated tubulin levels in Mfn2 KD neurons,

385   prevented both retraction bulb formation and axonal degeneration in neurons deprived of MFN2,

386   while having only negligible effects on WT controls (Fig. 5G-I).

387   These findings indicated that MFN2 dependent recruitment of ATAT1 to sites of

388   mitochondrial contacts with MTs is conserved in sensory neurons and required for axonal integrity

389   by maintaining normal levels of MT acetylation. Taking consideration of our functional data in

390   MEF cells, and consistent with previous observations in cellular models of CMT2 caused by

391   MFN2 mutations, these results also suggest that distal axonal degeneration caused by mutant

392   MFN2 predominantly depends on loss of acetylated tubulin, which affects mitochondrial motility

393   and distribution, but not on loss of fusion or functional mitochondria/ER tethering.

394

395

396

397

398

399

400

401

402

403

404

405

406

407

408

409

410

411

412

413

414

415

416

417

418

419

420

421

422

423

424

Main Text and Figures   Kumar et al.

Figure 4
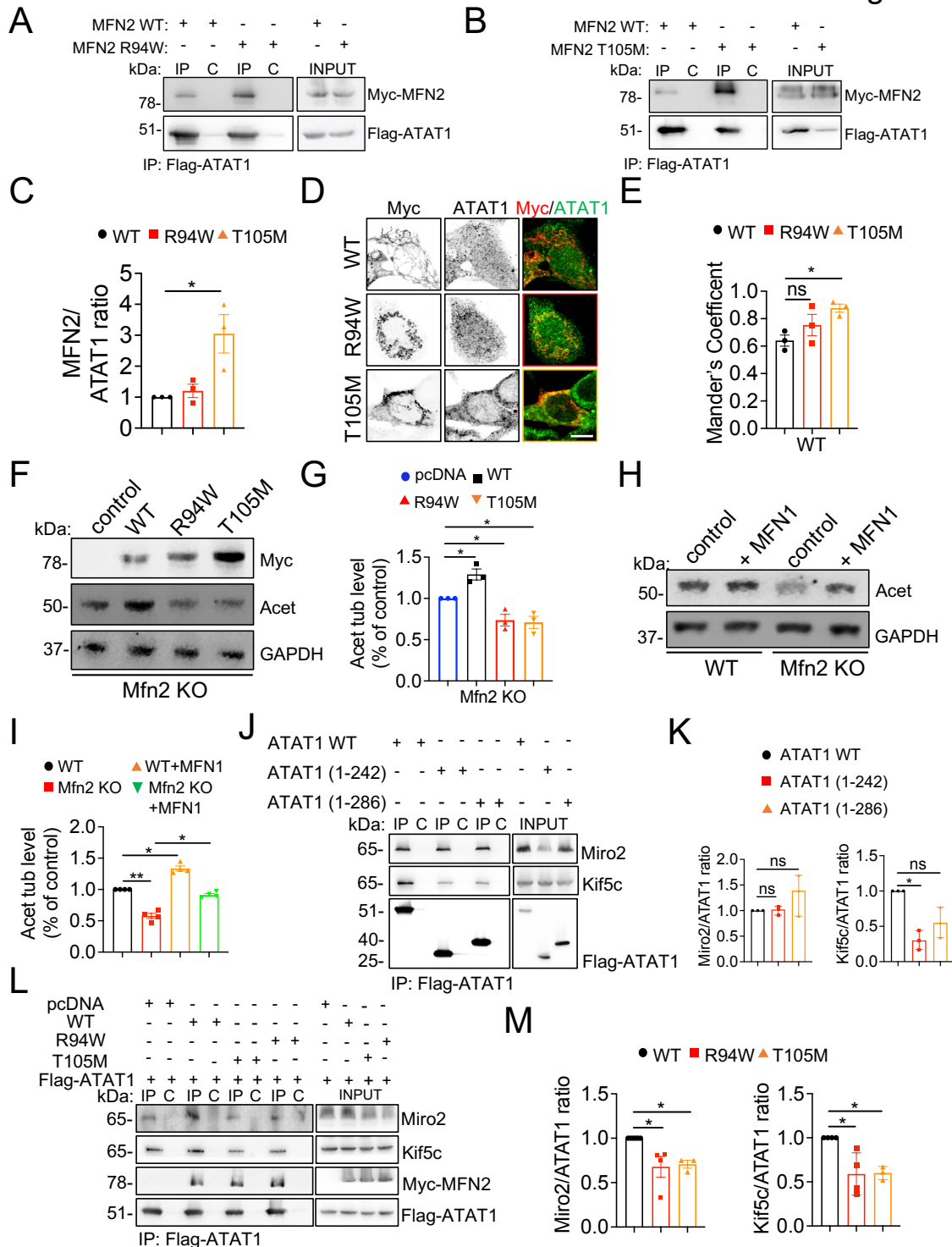

Figure 4. Regulation of α-tubulin acetylation by MFN2 is affected by MFN2 mutations and shared by MFN1. (A) HEK293T cells were co-transfected with Flag-ATAT1 and Myc-MFN2 WT or Myc-MFN2 R94W. (B) HEK293T cells were co-transfected with Flag-ATAT1 and Myc-MFN2 WT or Myc-MFN2 T105M. Interaction between ATAT1 WT and MFN2 WT or mutants was detected by immunoprecipitation (IP) followed

18

429   by immunoblot (IB) with the indicated antibodies. (C) The ratio of the MFN2 signal to the ATAT1 signal from

430   (A and B) was plotted. (D) Immunofluorescence analysis of overexpression of Myc-MFN2 WT, Myc-MFN2

431   R94W, Myc-MFN2 T105M in WT MEF cells (n=25-30 cells). (E) Mander's coefficient analysis for WT MEF

432   cells co transfected with Myc-MFN2 WT, Myc-MFN2 R94W and Myc-MFN2 T105M. (F) representative

433   immunoblot of acetylated tubulin levels in Mfn2 KO cells co-transfected with Myc-MFN2 WT, Myc-MFN2

434   R94W and Myc-MFN2 T105M. (G) Quantification of acetylated tubulin levels expressed as % of control levels

435   from 3 independent experiments as in F. (H) Representative immunoblot of acetylated tubulin levels in MFN1

436   overexpressing WT and Mfn2 KO cells. (I) Quantification of acetylated tubulin levels expressed as % of control

437   levels from 4 independent experiments as in H. (J) Interaction between ATAT1 or its truncated mutants (1-242;

438   1-286) and endogenous Miro2 or Kif5c was detected in HEK293T cells transfected with Flag-ATAT1 WT or its

439   truncated mutants. (K) The ratio of the Miro2 and Kif5c signal to the ATAT1 signal from (J) was plotted. (L)

440   Interaction between Flag-ATA1 and endogenous Miro2 or Kif5c was detected in HEK293T cells in presence or

441   absence of Myc-MFN2 WT, Myc-MFN2 R94W and Myc-MFN2 T105M. (M) The ratio of the Miro2 and Kif5c

442   signal to the ATAT1 signal from (L) is plotted. Data are expressed as median with interquartile range. n= 3-4

443   independent experiments. * p≤0.05, ** p<0.01; ns non-significant by Kruskal-Wallis test. Scale bar, 10 µm.

444

445

446

447

448

449

450

451

452

453

454

455

456

457

458

459

460
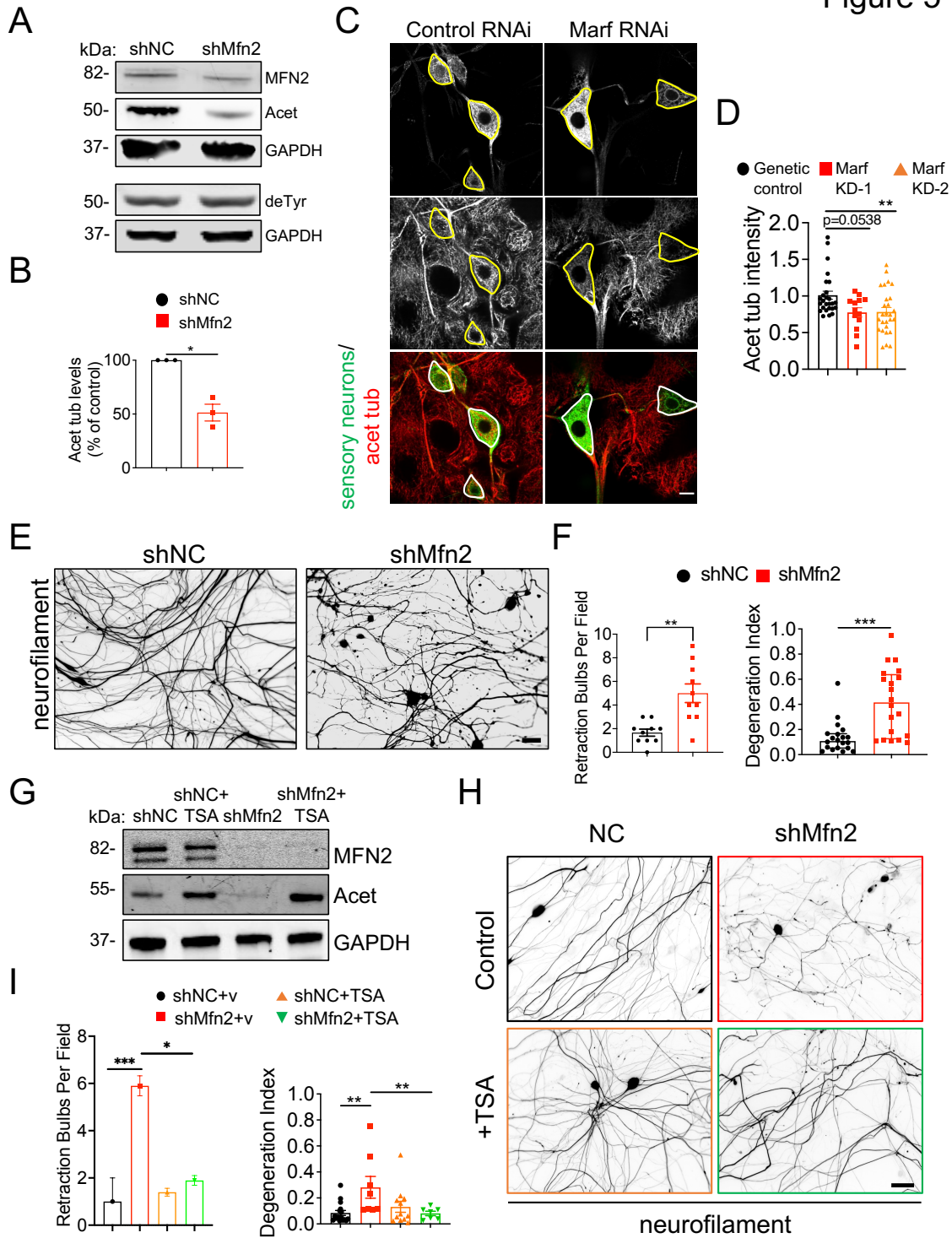
461

462

463

464

465

Figure 5. MFN2 regulates α-tubulin acetylation in sensory neurons in vitro and in vivo and this activity is required for axonal integrity. (A) Representative immunoblot of MFN2, acetylated (Acet) and detyrosinated

468   tubulin (deTyr) levels in adult DRG neurons (14 DIV) silenced of Mfn2 expression at 7 DIV. GAPDH, loading

469   control. (B) Quantification of acetylated tubulin relative in MFN2 depleted DRG neurons relative to control

470   neurons infected with shNC (non-coding shRNA). (C) Multi-dendritic neuron driver 109(2)80 Gal4 driver was

471   used to label somatosensory neurons (CD8-GFP) and knockdown (KD) Marf in *Drosophila* larval

472   somatosensory neurons. Acetylated tubulin levels were measured in the cell bodies as demarcated in the images.

473   Confocal stacks spanning the cell body were examined to reveal acetylated tubulin staining in cell bodies distinct

474   from nearby epidermis. To quantify levels of acetylated tubulin staining in cell bodies, images were sub-stacked

475   for each cell body (average intensity z-projection) and blinded. Mean gray value was measured and normalized

476   against the background level of acetylated tubulin staining (see methods for further information). (D)

477   Quantification of acetylated tubulin protein expression in cell bodies after Marf knockdown in somatosensory

478   neurons in larvae. Two different strategies were used, Marf KD-1 (BL 67158) and KD-2 (BL 31157). (E) Images

479   of representative fields showing dissociated adult DRG neurons (14 DIV) treated as in A, fixed and

480   immunostained with mouse anti-neurofilament (2H3-s) antibody. (F) Quantification of number of retraction

481   bulbs per field and degree of axonal degeneration. The area occupied by the axons (total axonal area) and

482   degenerating axons (fragmented axonal area) was measured in the same field from images in WT and MFN2

483   KD DRG neurons. Degeneration index was calculated as the ratio between fragmented axonal area and total

484   axonal area. (G) Representative immunoblot of MFN2, acetylated tubulin (Acet) levels in control (shNC) and

485   MFN2 (shMFN2) silenced DRG neurons incubated with 10 µM of the HDAC6 inhibitor TSA or vehicle control

486   for 6 h prior to lysis. GAPDH, loading control. (H) Representative immunofluorescence images of DRG neurons

487   treated as in G. (I) Quantification of number of retraction bulbs per field and degree of axonal degeneration in

488   DRG neurons treated as in G prior to fixation and staining. Data are represented as median and interquartile

489   range from 3 independent experiments. * $p<0.05$; ** $p<0.01$, *** $p<0.001$ by Mann-Whitney U test (B, D and

490   F) and Kruskal-Wallis test (I). Scale bars, 5 µm (C); 50 µm (H).

491

Discussion

493   MFN2 mutations in CMT2A disrupt the fusion [64] of mitochondria and compromise ER-

494   mitochondrial interactions [34, 47]. However, while certain CMT2A mutant forms of MFN2

495   impair mitochondrial fusion and/or functional mitochondria/ER tethering, others do not affect

496   either function [64], casting doubt on the implication of these MFN2 activities in the etiology of

497   CMT2.

498   In this study we report that MFN2 is a regulator of α-tubulin acetylation and MT dynamics,

499   and that in Mfn2 KO MEFs rescuing α-tubulin acetylation levels by pharmacological inhibition

500   of HDAC6 corrects defects in MT dynamics and mitochondrial motility, some MAM function

501   but not MAM integrity or mitochondrial fusion. We also show that regulation of tubulin

502 acetylation by MFN2 occurs through MFN2-mediated recruitment of ATAT1 to outer

503 mitochondrial membranes, an activity conserved in sensory neurons, critical in the induction of

504 axonal degeneration by MFN2 loss of function and impaired in two MFN2 mutants associated

505 with CMT2A. Interestingly, the binding of MFN2 to ATAT1 is dependent on the N-terminal

506 catalytic domain of ATAT1 and the same domain is also necessary for the association of

507 ATAT1 with kinesin-1 but not with miro, a Rho-GTPase implicated in the regulation of

508 mitochondrial transport by linking mitochondria outer membranes to kinesin and dynein motors

509 [65, 66]. Conversely, both MFN2 R94W and T105M mutants disrupt the binding of ATAT1 with

510 either miro or kinesin-1, suggesting that while ATAT1 binding to miro may not depend on kinesin,

511 the formation of a stable ATAT1/miro/kinesin-1 complex relies on functional MFN2. Based on

512 these observations, we propose that, in analogy to axonal vesicles [21], mitochondria contacts with

513 MTs are hotspots of tubulin acetylation and that this function is impaired in CMT2 disease caused

514 by MFN2 mutations. Specifically, we suggest that mutant MFN2 R94W or T105M drive axonal

515 degeneration by disrupting the ability of mitochondria to release the ATAT1 at specific sites on

516 axonal MTs, leading to an imbalance in tubulin acetylation and disrupted mitochondrial transport.

517 Our findings also provide evidence that the release of ATAT1 by MFN2 depends on the

518 formation of a stable ATAT1/miro/kinesin-1 complex, which may be necessary to allow

519 discharge of ATAT1 at putative entry sites into the MT lattice. This is in line with the

520 observation that motors can leave marks in the MT shaft by inducing breaks in the lattice and

521 promote MT self-repair [48, 50, 51]. Further work is required to understand the rules of site

522 selection and whether a break in the MT lattice is sufficient to induce ATAT1 release from

523 MFN2 through a putative conformational change in the motor complex.

524   By combining our observations in Mfn2 KO MEFs and KD sensory neurons, we propose

525 that axonal degeneration caused by MFN2 loss of function mutations may not depend on

526 impaired mitochondrial fusion or functional mitochondria/ER tethering, but rather loss of

527 MFN2-dependent regulation of mitochondrial transport by interfering with tubulin acetylation

528 at sites of mitochondria and MT contact. Our interpretation is consistent with a pathogenic role

529 for disrupted mitochondrial transport in neuropathies and a key role for tubulin acetylation in

530 mitochondrial dynamics. Indeed, multiple studies report that axonal degeneration precedes cell

531 body death in several peripheral neuropathies, including CMT disease. Mitochondria are the

532 principal mediators of ATP production and Ca^{2+} buffering, and they actively distribute to areas of

533 high energy demand and Ca^{2+} flux within the axon [43, 44]. A general defect in the ability of

534 mitochondria to translocate to these sites would be expected to lead to preferential degeneration of

535 long axons that frequently experience fluctuations in ATP and Ca^{2+} levels.

536 　　　Several lines of evidence further support a role for perturbation of acetylated tubulin levels

537 in CMT2A: 1) mutant MFN2 (MFN2R94Q) knock-in mice lack acetylated tubulin in distal axons

538 of their long peripheral nerves [29]; 2) HDAC6 inhibition has been reported to be a promising

539 therapeutical approach in several toxic and familial peripheral neuropathies, including CMT2A

540 [29]; 3) the formin INF2, mutations of which cause dominant intermediate CMT in association

541 with FSGS [67], is a positive regulator of tubulin acetylation by modulating ATAT1 transcription.

542 We note, however, that HDAC6 deacetylates additional lysine residues of α- and β-tubulin and has

543 multiple substrates in addition to tubulin, casting doubt on the specificity of this approach.

544 Conversely, tubulin is the only known substrate for ATAT1. In addition, the structure of ATAT1

545 provides a unique scaffold for designing small molecule modulators of tubulin acetylation for

546 therapeutic use [68]. In particular, the identification of ATAT1 mutations that decrease or increase

547 ATAT1 activity suggests that small molecule compounds could be identified to increase or

548 decrease ATAT1 activity to stabilize or destabilize MTs for therapeutic purposes [68]. Taken

549 together, these studies indicate that targeting ATAT1 activity or expression may represent an

550 alternative and more specific therapeutic approach aimed at restoring sensory neuron function in

551 CMT2A and perhaps other related CMT subtypes.

552

553 **MATERIALS AND METHODS**

REAGENT or RESOURCE	SOURCE	IDENTIFIER
Antibodies		
Mouse monoclonal mitofusin-2 (6A8)	Abcam	Ab56889
Rabbit monoclonal mitofusin-2	Abcam	Ab124773
Rabbit polyclonal IQGAP1	Novus Biologicals	NBP1-06529
Rabbit polyclonal HDAC6	Novus Biologicals	NBP1-78981
Rabbit polyclonal ATAT1	Bioss	Bs-9535R
Rabbit monoclonal TOMM20	Abcam	Ab186735

Mouse monoclonal TOMM20	Millipore Sigma	KB061-4F3
Rabbit polyclonal detyrosinated tubulin	Abcam	Ab48389
Rat tyrosinated tubulin, clone YL1/2	Millipore	MAB1864-I
Mouse monoclonal acetylated tubulin	Sigma Aldrich	T6793
Mouse monoclonal DM1A	Sigma Aldrich	T6199
Human anti-tubulin GTP (MB11)	Adipogen	AG-27B-0009-C100
Rabbit polyclonal TTL	Proteintech	13618-1-AP
Mouse monoclonal PDI	Santacruz	SC-74551
Mouse monoclonal anti-c-Myc 9E10 HRP	Santacruz	SC-40 HRP
Mouse monoclonal anti-c-Myc 9E10 Agarose	Santacruz	SC-40 AC
Mouse monoclonal anti-Flag M2 HRP	Sigma Aldrich	A8592
Mouse monoclonal anti-Flag M2 Agarose	Sigma Aldrich	A2220
Chicken polyclonal neurofilament	Aves labs	AB_2313553
Rabbit polyclonal anti-Miro2	Proteintech	11235-1-AP
Rabbit polyclonal anti-Kif5c	Proteintech	25897-1-AP
Mouse monoclonal GAPDH	Abcam	Ab8245
Rabbit polyclonal GAPDH	ThermoFisher	PA1-987
Goat anti-mouse IgG (H+L) highly cross-adsorbed secondary antibody, Alexa Flour 488-conjugated	ThermoFisher	A11029
Goat anti-rabbit IgG (H+L) highly cross-adsorbed secondary antibody, Alexa Flour 488-conjugated	ThermoFisher	A11034
Goat anti-mouse IgG (H+L) highly cross-adsorbed secondary antibody, Alexa Flour 546-conjugated	ThermoFisher	A11030
Goat anti-rabbit IgG (H+L) highly cross-adsorbed secondary antibody, Alexa Flour 546-conjugated	ThermoFisher	A11035
Goat anti-human IgG (H+L) highly cross-adsorbed secondary antibody, Alexa Flour 568-conjugated	ThermoFisher	A-21090
IRDye® 680RD Goat anti-mouse IgG secondary antibody	LI-COR	926-68070

IRDye® 800CW Goat anti-rabbit IgG secondary antibody	LI-COR	926-32211
IRDye® 680RD Goat anti-rabbit IgG secondary antibody	LI-COR	926-68071
IRDye® 800CW Goat anti-rabbit IgG secondary antibody	LI-COR	926-32211
Bacteria strains		
DH5 alpha	New England Biolabs	C2987I
XL1-Blue	Agilent	200229
Chemicals and Reagents		
Trichostatin A (TSA)	Tocris	#1406
Tubacin	Millipore Sigma	SML0065
Mitotracker Red CMXROS	Thermofisher	M7512
DMEM	Gibco	11995-065
Neurobasal	Thermofisher	110349
Fetal bovine serum	HyClone	SH30071.03
Bovine calf serum	Thermofisher	26170043
B-27 supplement (50x)	Thermofisher	7504044
Penicillin-streptomycin	Thermofisher	15140163
10x HBSS	Thermofisher	14065056
Cytosine β-D-arabinofuranoside hydrochloride (AraC)	Millipore Sigma	C6645
Collagenase	Millipore Sigma	C0130
Trypsin 0.05% EDTA	Thermofisher	25300054
GlutaMAX Supplement	Thermofisher	35050061
Poly-D-Lysine	Sigma Aldrich	P1149
Laminin	Sigma Aldrich	11243217001
Laemlli SDS sample buffer, reducing	Thermofisher	J60015-AD

NuPAGE MOPS SDS Running buffer	Thermofisher	NP0001
Fluoromount-G	Southern Biotech	0100-01
32% PFA	EMS	15714-S
DreamFect^{TM}Gold transfection reagent	OZ Bioscience	DG80500
c-Myc Peptide	Sigma Aldrich	M2435
Flag peptide	Sigma Aldrich	F3290
Critical commercial assays		
DuoLink PLA In Situ Red starter mouse/rabbit kit	Sigma-Aldrich	DUO92101
Experimental models: Organisms/strains		
UAS-MARF RNAi	Bloomington Stock Center	BL 31157
UAS-MARF miRNA CDS	Bloomington Stock Center	BL 67158
Mouse: C57BL/6J	Charles River Laboratories	RRID:IMSR_CRL:027
Recombinant DNA		
pLKO.1 shMfn2	Sigma Aldrich	TRCN0000080608
pLKO.1 shTTL	Sigma Aldrich	TRCN0000191515
Myc-MFN2 WT	David Chan	NA
Myc-MFN2 R94W	David Chan	NA
Myc-MFN2 T105M	David Chan	NA
Flag-ATAT1 WT	Laurent Ngyuen	NA
Flag-ATAT1 (1-242)	Laurent Ngyuen	NA
Flag-ATAT1 (1-286)	Laurent Ngyuen	NA
Zsgreen-MFN1	Estella Area Gomez	NA
Software		
ImageJ (Fiji)	NIH	RRID:SCR_002285

GraphPad Prism	GraphPad	RRID:SCR_002798
Li-COR Image Studio Software	Li-COR	RRID:SCR_015795
Zeiss ZEN	Zeiss	RRID:SCR_013672
Andor iQ3	Oxford Instruments	RRID:SCR_014461
Other		
18 mm No.1 circle coverglass	Carolina	633033
35 mm MatTek dishes	MatTek	P35G-1.5-14-C
NuPAGE Gel	ThermoFisher	NP0316
Nitrocellulose membrane	Fisher	10600011

554

Lead contact and materials availability

Further information and requests for resources and reagents should be directed to and will be fulfilled by the lead contact, Francesca Bartolini (fb2131@columbia.edu).

Experimental model and subject details

All protocols and procedures for mice were approved by the Committee on the Ethics of Animal Experiments of Columbia University and according to Guide for the Care and Use of Laboratory Animals of the National Institutes of Health.

Cell culture and analyses

WT, Mfn2 KO, Mfn1 KO (kind gifts of Dr. Area-Gomez) and Iqgap1 KO mouse embryonic fibroblast cells were grown in DMEM supplemented with 10% fetal bovine serum. Cells were grown to 80% confluency on acid treated glass coverslips prior to experiment.

Immunofluorescence microscopy and analyses

568

569 For immunofluorescence staining of the MT cytoskeleton, cells were fixed in ice cold MetOH for

570 10' prior to rehydration in PBS buffer o/n at 4°C. For all other stainings, cells were fixed in 4%

571 PFA for 15 min and permeabilized with 0.1% Triton X-100 for 5 min at R.T. Cells were then

572 washed in PBS, blocked in 2% FBS and 2% BSA in PBS for 1 h, stained with primary antibodies

573 overnight at 4ºC followed by secondary antibodies for 1 h. Mounted samples were observed using

574 a Zeiss LSM 800 confocal microscope equipped with Airyscan module, using a 63x objective

575 (Plan-Apochromat, NA 1.4). Images were acquired and processed using Zen Blue 2.1 software.

576 All images were analyzed by ImageJ software.

577

Western blot analyses

578

579 Cells were lysed in Laemmli sample buffer and boiled at 96ºC for 5 min. Cell lysates were

580 sonicated with a probe sonicator to sheer cellular debris and genomic DNA. Proteins were

581 separated by 10% Bis-Tris gel (Invitrogen) and transferred onto nitrocellulose membrane. After

582 blocking in 5% milk/TBS or BSA/TBS, membranes were incubated with primary antibodies at

583 4ºC overnight prior to 1 h incubation with secondary antibodies. Image acquisition was performed

584 with an Odyssey imaging system (LI-COR Biosciences, NE) and analyzed with Odyssey software.

585

Proximity ligation assay (PLA)

586

587 PLA assays were carried out using a Duolink *in situ* red starter kit mouse/rabbit kit (Sigma-

588 Aldrich) according to the manufacturer's protocol. The primary antibodies used were mouse anti-

589 MFN2 and rabbit anti-ATAT1 (1:1000 dilution). Images were acquired on a Zeiss LSM

590 800 confocal microscope and analyzed using ImageJ/FIJI. Data were pulled from at least three

591 independent biological repeats.

592

Analysis of mitochondrial morphology, motility and distribution

593

594 Mitochondria were labeled using mitotracker Red CMROX according to manufacturer protocol

595 (Thermo Fisher Scientific) and detected by epifluorescence microscope equipped with 60 x

596 objective lens (Olympus IX81) and a monochrome CCD camera (Sensicam QE, Cooke

597 Corporation). Aspect ratio (length/width) were measured using Image J/FIJI. For mitochondrial

598 distribution and displacement velocity mitochondria were live imaged for 3 min at 2 sec/frame at

599   37°C. A customized Mitoplot software (kind gift of Dr. Gregg Gundersen) was used for analyzing

600   mitochondrial distribution. Manual tracking plug-in in ImageJ/FIJI was used to analyze

601   mitochondrial displacement velocity.

602

603   **Microtubule dynamics**

604   Fibroblasts were transfected with pMSCV-puro-tagGFP-C4 α-tubulin plasmid to generate a green

605   fluorescent protein (GFP)–tubulin stably expressing cell line. Live imaging of MT dynamics in

606   transfected cells was performed at 37°C and 5% CO_2 for 5 min (5 s/frame) with a 100× PlanApo

607   objective (numerical aperture 1.45) and an iXon X3 CCD camera (Andor, Belfast, United

608   Kingdom) on a Nikon Eclipse Ti microscope controlled by Nikon's NIS-Elements software

609   (Nikon, Tokyo, Japan). Movies were analyzed by ImageJ using a manual tracking plug-in.

610

611   **Mitodendra**

612   Dendra2 photoconversion and imaging utilized the protocol from Evrogen. Images were acquired

613   with an Olympus spinning disk microscope EC-Plan-Neofluar 40X/1.3 oil. Z-stack acquisitions

614   over-sampled each optical slice twice, and the Zen 2009 image analysis software was used for

615   maximum z-projections. The 488 nm laser line and the 561 nm laser excited Dendra2 in the

616   unconverted state and photo-converted state, respectively. To photo-switch Dendra2, a region was

617   illuminated with the 405 nm line (4% laser power) for 90 bleaching iterations.

618

619   **Lentivirus production**

620   Production of lentiviral particles was conducted using the second-generation packaging system as

621   previously described [69, 70]. In brief, HEK293T cells were co-transfected with lentiviral plasmid

622   shRNA and the packaging vectors pLP1, pLP2, and pLP-VSV-G (Thermo Fisher) using the Ca^{2+}

623   phosphate transfection method. At 24, 36, and 48 h after transfection, the virus-containing

624   supernatant was collected, and the lentiviral particles concentrated (800-fold) by

625   ultracentrifugation (100,000 × g at 4 °C for 2 h) prior to aliquoting and storage at −80 °C.

626

627   **MT stability**

628   WT and Mfn2 KO MEFs were incubated at 8 °C for 30 min to induce mild microtubule

629   depolymerization. At the end of the incubation time, cells were gently washed with PEM 1× buffer

630   (85 mM Pipes, pH 6.94, 10 mM EGTA, and 1 mM $MgCl_2$) twice before extraction with PEM

631   buffer, supplemented with 0.05 % Triton X-100. After 1 min extraction at 8 °C, a matching volume

632   of fixative buffer (ice cold MetOH) was added dropwise to the coverslips, and cells were incubated

633   for another 5 min at -20 °C. Cells were finally washed with PBS 1× and processed for

634   immunofluorescence labeling. All images were analyzed using ImageJ software [71].

635

Analysis of phospholipid synthesis in cultured cells

637   Both mitochondria and ER play key roles in the synthesis of phosphatidylserine (PtdSer),

638   phosphatidylethanolamine (PtdEtn), and phosphatidylcholine (PtdCho). PtdSer is synthesized in

639   the MAM; it then translocates to mitochondria, where it is converted to PtdEtn; PtdEtn then

640   translocates back to the MAM, to generate PtdCho[72]. To test the effect of MFN2 on phospholipid

641   synthesis mediated by MAM, WT and Mfn2 KO MEF cells were incubated for 2 h with serum-

642   free medium to ensure removal of exogenous lipids. The medium was then replaced with MEM

643   containing 2.5 µCi/ml of ^{3}H-serine for 2, 4 and 6 h. The cells were washed and collected in DPBS,

644   pelleted at 2500 g for 5 min at 4ºC, and resuspended in 0.5 ml water, removing a small aliquot for

645   protein quantification. Lipid extraction was done by the Bligh and Dyer method. Briefly, three

646   volumes of chloroform/methanol 2:1 were added to the samples and vortexed. After centrifugation

647   at 8000 g for 5 min, the organic phase was washed twice with two volumes of methanol/water 1:1,

648   and the organic phase was blown to dryness under nitrogen. Dried lipids were resuspended in 60

649   µl of chloroform/methanol 2:1 (v/v) and applied to a TLC plate. Phospholipids were separated

650   using two solvents, composed of petroleum ether/diethyl ether/acetic acid 84:15:1 (v/v/v) and

651   chloroform/methanol/acetic acid/water 60:50:1:4 (v/v/v/v). Development was performed by

652   exposure of the plate to iodine vapor. The spots corresponding to the relevant phospholipids

653   (identified using co-migrating standards) were scraped and counted in a scintillation counter

654   (Packard Tri-Carb 2900TR). Both mitochondria and ER play key roles in the synthesis of

655   phosphatidylserine (PtdSer), phosphatidylethanolamine (PtdEtn), and phosphatidylcholine

656   (PtdCho). PtdSer is synthesized in the MAM; it then translocates to mitochondria, where it is

657   converted to PtdEtn; PtdEtn then translocates back to the MAM, to generate PtdCho [73].

658   Therefore, to test directly the effect of MFN2 mutations on phospholipid synthesis mediated by

659   MAM, we incubated control and Mfn2 KO fibroblasts in medium containing ^{3}H-serine and

660   measured the incorporation of the label into newly-synthesized ^{3}H-PtdSer and ^{3}H-PtdEtn after 2

661   and 4 h.

662

663   **Lipidomics**

664   All samples were collected and treated following recently accepted guidelines for the analysis of

665   human blood plasma and/or serum. Lipids were extracted from equal amounts of material (0.2

666   ml/sample) by a chloroform–methanol extraction method. Three comprehensive panels, scanning

667   for either positive lipids, negative lipids or neutral lipids (under positive mode), were analyzed.

668   Equal amounts of internal standards with known concentrations were spiked into each extract.

669   Each standard was later used to calculate the concentrations of corresponding lipid classes by first

670   calculating ratio between measured intensities of a lipid species and that of corresponding internal

671   standard multiplied by the known concentration of the internal standard. Samples were analyzed

672   using a 6490 Triple Quadrupole LC/MS system (Agilent Technologies, Santa Clara, CA).

673   Cholesterol and cholesterol esters were separated with normal-phase HPLC using an Agilent

674   Zorbax Rx-Sil column (inner diameter 2.1 Å~ 100 mm) under the following conditions: mobile

675   phase A (chloroform:methanol:1 M ammonium hydroxide, 89.9:10:0.1, v/v/v) and mobile phase

676   B (chloroform:methanol:water: ammonium hydroxide, 55:39.9:5:0.1, v/v/v/v); 95% A for 2 min,

677   linear gradient to 30% A over 18 min and held for 3 min, and linear gradient to 95% A over 2 min

678   and held for 6 min.

INTERNAL STANDARD	Corresponding Lipid Class	Concentration (ug/ul)
IS AcylPG 14:0-28:0	Acyl PG, NAPE, NAPS	0.046799614
IS BMP 28:0	BMP	0.015298133
IS CE C17	CE	78.59098931
IS Cer C17:0	Cer, dhCer	0.758320608
IS Chol d7 b	Free Cholesterol	63.78791732

IS DG 4ME	diacylglycerols	0.640874053
IS dhSM d18:0/12:0	dihydrosphingomyelins	2.579623778
IS DMPC	AC	12.34642208
IS GalCer d18:1/12:0	MhCer	1.039897431
IS LacCer d18:1/12:0	LacCer	0.259594347
IS LPC 13:0	LPC	12.34642208
IS LPE 14:0	LPE	0.098349468
IS LPI 13:0	LPI	0.07642123
IS MG C17	MG	0.242952978
IS PA 28:0	PA	0.068072997
IS PC 28:0	PC	12.34642208
IS PE 25:0	PE	8.839285714
IS PG 12:0/13:0	PG	0.446428571
IS PI 12:0/13:0	PI	2.232142857
IS PS 28:0	PS	11.92531331
IS SM d18:1/12:0	SM	13.39285714
IS Sulf d18:1/12:0	Sulf	0.225924621
IS TG 50:0 d5	TG	0.498018035

679

680

Cellular fractionation

681

682   WT and Mfn2 KO fibroblasts were cultured on 15 cm petri dishes. Buffer A (10mM HEPES, 1.5

683   mM $MgCl_2$, 10 mM KCl, 0.5 mM DTT, 0.05% NP40, pH 7.9) was prepared freshly and protease

684   and phosphatase inhibitors were added. Cells were scraped thoroughly using buffer A and left on

685   ice for 10 min. Samples were centrifuged at 3000 rpm for 10 min at 4°C and supernatants stored

686   on ice. Pellets were resuspended in buffer B (5 mM HEPES, 1.5 mM $MgCl_2$, 0.2 mM EDTA, 0.5

687   mM DTT, 26% Glycerol (v/v), pH 7.9) and added 4.6 M NaCl. Homogenize with 20 full stroke of

688   Dounce homogenizer on ice and leave it on ice for 30 min.

689

Isolation of adult DRG neurons

690

691   DRG were dissected from 8- to 10-wk-old C57BL/6J mice in cold Hank's balanced salt solution

692   (HBSS) (Life Technologies) or Dulbecco's Modified Eagle's medium (Life Technologies) and

693   dissociated in 1 mg/mL Collagenase A for 1 h at 37 °C, followed by 0.05% trypsin (Life

694   Technologies) digestion for 3 to 5 min at 37 °C and washed with Neurobasal medium (Invitrogen)

695   supplemented with 2% B-27 (Invitrogen), 0.5 mM glutamine (Invitrogen), fetal bovine serum

696   (FBS), and 100 U/mL penicillin-streptomycin. DRG neurons were then triturated by repeated

697   gentle pipetting until no clump was visible, and neuronal bodies were resuspended in Neurobasal

698   medium with FBS prior to plating onto 12 well plates (over 18 mm coverslips) that had been coated

699   overnight with 100 μg/ mL poly-D-lysine at 37 °C and for 1 h at 37 °C with 10 μg/mL laminin

700   (Life Technologies). After 30 min, Neurobasal medium, without FBS, was added to the plate. At

701   4 DIV, at least 30% of media was changed and 10 μM AraC was added to media every 4 d.

702

Degeneration index in DRG neurons

703

704   As reported previously [69], images of an average of 10 random fields of dissociated adult DRG

705   neurons fixed and immunostained with mouse anti-neurofilament antibody were acquired using a

706   20× objective lens (Olympus IX81) coupled to a monochrome CCD camera (Sensicam QE; Cooke

707   Corporation). To quantify axonal degeneration, the areas occupied by the axons (total axonal area)

708   and degenerating axons (fragmented axonal area) were measured in the same field from images of

709   DRG neurons. Images were automatically thresholded (global threshold) using a default auto

710   threshold method, binarized, and the fragmented axonal area measured by using the particle

711   analyzer module of ImageJ (size of small fragments = 20 to 10,000 pixels). Degeneration index

712   was calculated as the ratio between the fragmented axonal area and the total axonal area.

713

714   **Immunolabeling of *Drosophila* larvae**

715   Immunolabeling of *Drosophila* larvae was performed largely as described previously [74]. Briefly,

716   late third instar larvae were dissected in $1 \times$ PBS, fixed in 4% paraformaldehyde (PFA, Electron

717   Microscopy Sciences) in $1 \times$ PBS for 15 min, washed three times in $1 \times$ PBS + 0.3% Triton X-100

718   (PBS-TX), and blocked for 1h at room temperature (RT) or overnight at 4 °C in 5% normal donkey

719   serum (NDS) in PBS-TX (Jackson Immunoresearch). Primary antibodies were chicken anti-GFP

720   (1:1000; Abcam) and acetylated alpha-tubulin (1:400; Sigma Aldrich) diluted in 5% NDS in PBS-

721   TX. The tissue was incubated overnight in primary antibodies at 4 °C and then washed in PBS-TX

722   for 3×15 min at RT. Species-specific, fluorophore-conjugated secondary antibodies (Jackson

723   ImmunoResearch) were used at 1:1000 in 5% NDS in PBS-TX and incubated overnight 4 °C.

724   Tissue was washed in PBS-TX for 3×15 min. Immunolabeled tissue was mounted on poly-L-

725   lysine coated coverslips, dehydrated 5 minutes each in an ascending ethanol series (30, 50, 70, 95,

726   2×100%), cleared in xylenes (2×10 min), and mounted in DPX (Fluka).

727

728   **Imaging and quantification of *Drosophila* sensory neurons**

729   Images of somatosensory neurons from *Drosophila* larvae were acquired using a Yokogawa CSU-

730   W1 SoRa mounted on a Zeiss Axio Observer using a 60x 1.46 NA Alpha Plan-Apochromat oil

731   objective and a 4x magnification changer. Acquisitions included the cell body, axon, and dendrites

732   of somatosensory neurons. Subsequent image analysis was performed using Fiji. Using the md

733   neurons (109(80)2-Gal4, UAS-CD8-GFP) as reference, sub stacks covering the z-depth of each

734   cell body were cropped and blinded for subsequent analysis. Additionally, 2-3 areas (300 x 300

735   px) devoid of neurons in the same image were selected to measure background levels of acetylated

736   tubulin in each image and used to normalize the levels in the cell body. To measure acetylated

737   tubulin levels in the cell bodies, cell bodies were selected using the polygon selection tool, and the

738   area outside the cell body was cleared to avoid including acetylated tubulin staining surrounding

739   the cell body in the subsequent quantification. Processed z-stacks of cell bodies were z-projected

740   using average intensity. The mean gray value was measured and normalized against background

741   levels of acetylated tubulin quantified in the same image. Raw images were used for quantification.

742   Represented images shown in Fig. 5C were deconvolved using Microvolution (20 iterations).

743

Co-immunoprecipitation assay

745   HEK293T cells were cultured in Dulbecco's modified Eagle's medium plus 10% fetal bovine

746   serum (FBS), penicillin–streptomycin (1%) and L-glutamine (1%). Transient transfections were

747   performed using DreamFect™Gold transfection reagent (Oz Biosciences SAS, Marseille, FR) in

748   accordance with the manufacturer's protocols. HEK293T cells were lysed in RIPA buffer (50 mM

749   Tris-HCl at pH 7.6, 150 mM NaCl, 0.5% sodium deoxycholic, 5 mM EDTA, 0.1% SDS, 100 mM

750   NaF, 2 mM NaPPi, 1% NP-40) supplemented with protease and phosphatase inhibitors, then

751   centrifuged at 13,000 rpm for 30 min at 4 °C and the resulting supernatants were subjected to

752   Bradford protein assay (Bio-Rad, Hercules, California, USA) for measuring total protein

753   concentration. Immunoprecipitations were performed on 1mg of whole cell extracts by using anti-

754   c-Myc agarose coniugated or anti-Flag M2 agarose (1–2 μg) for 2 h at 4 °C with rotation. c-Myc

755   peptide or Flag-peptide (0,1 mg/ml) was used as a control. The immunoprecipitates were then

756   washed five times with RIPA buffer, resuspended in sample loading buffer, boiled for 5 min,

757   resolved in sodium dodecyl sulphate–polyacrylamide gel electrophoresis (SDS-PAGE), and then

758   subjected to immunoblot analysis.

759

Quantification and statistical analysis

761   Data are shown as median with interquartile range from at least 3 independent experiments and

762   figures are generated by GraphPad Prism. Image analysis was performed by ImageJ (Fiji).

763   Statistical analysis between two groups was performed Mann-Whitney U test and among 3 or more

764   groups was performed using the Kruskal-Wallis with Dunn's multiple comparisons test. Data are

765   shown as means ±SEM, and statistical significance was analyzed by student's t test (Table1) and

766   two-way ANOVA with Dunnett's multiple comparison (Table S1 and S2).

767

Acknowledgements

772   stimulating discussions and access to his microscopes, and to Laurent Nguyen for sharing his

773   ATAT1 constructs. Figures were prepared using PowerPoint and BioRender.

774

References

776   1.   Goodson, H.V. and E.M. Jonasson, *Microtubules and Microtubule-Associated Proteins.*
777   Cold Spring Harb Perspect Biol, 2018. **10**(6).
778   2.   Kapitein, L.C. and C.C. Hoogenraad, *Building the Neuronal Microtubule Cytoskeleton.*
779   Neuron, 2015. **87**(3): p. 492-506.
780   3.   Baas, P.W., et al., *Polarity orientation of microtubules in hippocampal neurons: uniformity*
781   *in the axon and nonuniformity in the dendrite.* Proc Natl Acad Sci U S A, 1988. **85**(21): p.
782   8335-9.
783   4.   Goldstein, L.S. and Z. Yang, *Microtubule-based transport systems in neurons: the roles of*
784   *kinesins and dyneins.* Annu Rev Neurosci, 2000. **23**: p. 39-71.
785   5.   Magiera, M.M., et al., *Tubulin Posttranslational Modifications and Emerging Links to*
786   *Human Disease.* Cell, 2018. **173**(6): p. 1323-1327.
787   6.   Pero, M.E., F. Chowdhury, and F. Bartolini, *Role of tubulin post-translational*
788   *modifications in peripheral neuropathy.* Exp Neurol, 2023. **360**: p. 114274.
789   7.   Portran, D., et al., *Tubulin acetylation protects long-lived microtubules against mechanical*
790   *ageing.* Nat Cell Biol, 2017. **19**(4): p. 391-398.
791   8.   Eshun-Wilson, L., et al., *Effects of alpha-tubulin acetylation on microtubule structure and*
792   *stability.* Proc Natl Acad Sci U S A, 2019. **116**(21): p. 10366-10371.
793   9.   Janke, C. and G. Montagnac, *Causes and Consequences of Microtubule Acetylation.* Curr
794   Biol, 2017. **27**(23): p. R1287-R1292.
795   10. Barlan, K. and V.I. Gelfand, *Intracellular transport: ER and mitochondria meet and greet*
796   *along designated tracks.* Curr Biol, 2010. **20**(19): p. R845-7.
797   11. Rowland, A.A. and G.K. Voeltz, *Endoplasmic reticulum-mitochondria contacts: function*
798   *of the junction.* Nat Rev Mol Cell Biol, 2012. **13**(10): p. 607-25.
799   12. Tran, A.D., et al., *HDAC6 deacetylation of tubulin modulates dynamics of cellular*
800   *adhesions.* J Cell Sci, 2007. **120**(Pt 8): p. 1469-79.
801   13. Valenzuela-Fernandez, A., et al., *HDAC6: a key regulator of cytoskeleton, cell migration*
802   *and cell-cell interactions.* Trends Cell Biol, 2008. **18**(6): p. 291-7.
803   14. Akella, J.S., et al., *MEC-17 is an alpha-tubulin acetyltransferase.* Nature, 2010. **467**(7312):
804   p. 218-22.
805   15. Shida, T., et al., *The major alpha-tubulin K40 acetyltransferase alphaTAT1 promotes rapid*
806   *ciliogenesis and efficient mechanosensation.* Proc Natl Acad Sci U S A, 2010. **107**(50): p.
807   21517-22.
808   16. L'Hernault, S.W. and J.L. Rosenbaum, *Chlamydomonas alpha-tubulin is*
809   *posttranslationally modified by acetylation on the epsilon-amino group of a lysine.*
810   Biochemistry, 1985. **24**(2): p. 473-8.
811   17. LeDizet, M. and G. Piperno, *Identification of an acetylation site of Chlamydomonas alpha-*
812   *tubulin.* Proc Natl Acad Sci U S A, 1987. **84**(16): p. 5720-4.
813   18. Schaedel, L., et al., *Microtubules self-repair in response to mechanical stress.* Nat Mater,
814   2015. **14**(11): p. 1156-63.

815   19.   Howes, S.C., et al., *Effects of tubulin acetylation and tubulin acetyltransferase binding on*
816   *microtubule structure.* Mol Biol Cell, 2014. **25**(2): p. 257-66.
817   20.   Coombes, C., et al., *Mechanism of microtubule lumen entry for the alpha-tubulin*
818   *acetyltransferase enzyme alphaTAT1.* Proc Natl Acad Sci U S A, 2016. **113**(46): p. E7176-
819   E7184.
820   21.   Even, A., et al., *ATAT1-enriched vesicles promote microtubule acetylation via axonal*
821   *transport.* Sci Adv, 2019. **5**(12): p. eaax2705.
822   22.   Ly, N., et al., *alphaTAT1 controls longitudinal spreading of acetylation marks from open*
823   *microtubules extremities.* Sci Rep, 2016. **6**: p. 35624.
824   23.   Montagnac, G., et al., *alphaTAT1 catalyses microtubule acetylation at clathrin-coated pits.*
825   Nature, 2013. **502**(7472): p. 567-70.
826   24.   Kalebic, N., et al., *alphaTAT1 is the major alpha-tubulin acetyltransferase in mice.* Nat
827   Commun, 2013. **4**: p. 1962.
828   25.   Morley, S.J., et al., *Acetylated tubulin is essential for touch sensation in mice.* Elife, 2016.
829   **5**.
830   26.   Yan, C., et al., *Microtubule Acetylation Is Required for Mechanosensation in Drosophila.*
831   Cell Rep, 2018. **25**(4): p. 1051-1065 e6.
832   27.   Van Helleputte, L., et al., *Inhibition of histone deacetylase 6 (HDAC6) protects against*
833   *vincristine-induced peripheral neuropathies and inhibits tumor growth.* Neurobiol Dis,
834   2018. **111**: p. 59-69.
835   28.   d'Ydewalle, C., et al., *HDAC6 inhibitors reverse axonal loss in a mouse model of mutant*
836   *HSPB1-induced Charcot-Marie-Tooth disease.* Nat Med, 2011. **17**(8): p. 968-74.
837   29.   Picci, C., et al., *HDAC6 inhibition promotes alpha-tubulin acetylation and ameliorates*
838   *CMT2A peripheral neuropathy in mice.* Exp Neurol, 2020. **328**: p. 113281.
839   30.   Morena, J., A. Gupta, and J.C. Hoyle, *Charcot-Marie-Tooth: From Molecules to Therapy.*
840   Int J Mol Sci, 2019. **20**(14).
841   31.   Feely, S.M., et al., *MFN2 mutations cause severe phenotypes in most patients with CMT2A.*
842   Neurology, 2011. **76**(20): p. 1690-6.
843   32.   Dorn, G.W., 2nd, *Mitofusin 2 Dysfunction and Disease in Mice and Men.* Front Physiol,
844   2020. **11**: p. 782.
845   33.   Filadi, R., D. Pendin, and P. Pizzo, *Mitofusin 2: from functions to disease.* Cell Death Dis,
846   2018. **9**(3): p. 330.
847   34.   Larrea, D., et al., *MFN2 mutations in Charcot-Marie-Tooth disease alter mitochondria-*
848   *associated ER membrane function but do not impair bioenergetics.* Hum Mol Genet, 2019.
849   **28**(11): p. 1782-1800.
850   35.   Baloh, R.H., et al., *Altered axonal mitochondrial transport in the pathogenesis of Charcot-*
851   *Marie-Tooth disease from mitofusin 2 mutations.* J Neurosci, 2007. **27**(2): p. 422-30.
852   36.   Schiavon, C.R., G.S. Shadel, and U. Manor, *Impaired Mitochondrial Mobility in Charcot-*
853   *Marie-Tooth Disease.* Front Cell Dev Biol, 2021. **9**: p. 624823.
854   37.   Palau, F., et al., *The role of mitochondrial network dynamics in the pathogenesis of*
855   *Charcot-Marie-Tooth disease.* Adv Exp Med Biol, 2009. **652**: p. 129-37.
856   38.   Cosson, P., et al., *Mitofusin-2 independent juxtaposition of endoplasmic reticulum and*
857   *mitochondria: an ultrastructural study.* PLoS One, 2012. **7**(9): p. e46293.
858   39.   Filadi, R., et al., *Mitofusin 2 ablation increases endoplasmic reticulum-mitochondria*
859   *coupling.* Proc Natl Acad Sci U S A, 2015. **112**(17): p. E2174-81.

860 40. Filadi, R., P. Theurey, and P. Pizzo, *The endoplasmic reticulum-mitochondria coupling in*
861   *health and disease: Molecules, functions and significance.* Cell Calcium, 2017. **62**: p. 1-
862   15.
863 41. Han, S., et al., *The role of Mfn2 in the structure and function of endoplasmic reticulum-*
864   *mitochondrial tethering in vivo.* J Cell Sci, 2021. **134**(13).
865 42. Bassot, A., et al., *Loss and gain of function of Grp75 or mitofusin 2 distinctly alter*
866   *cholesterol metabolism, but all promote triglyceride accumulation in hepatocytes.* Biochim
867   Biophys Acta Mol Cell Biol Lipids, 2021. **1866**(12): p. 159030.
868 43. Misko, A., et al., *Mitofusin 2 Is Necessary for Transport of Axonal Mitochondria and*
869   *Interacts with the Miro/Milton Complex.* Journal of Neuroscience, 2010. **30**(12): p. 4232-
870   4240.
871 44. Misko, A.L., et al., *Mitofusin2 mutations disrupt axonal mitochondrial positioning and*
872   *promote axon degeneration.* J Neurosci, 2012. **32**(12): p. 4145-55.
873 45. Mou, Y., et al., *MFN2 Deficiency Impairs Mitochondrial Transport and Downregulates*
874   *Motor Protein Expression in Human Spinal Motor Neurons.* Front Mol Neurosci, 2021.
875   **14**: p. 727552.
876 46. Zhou, Y., et al., *Restoring mitofusin balance prevents axonal degeneration in a Charcot-*
877   *Marie-Tooth type 2A model.* J Clin Invest, 2019. **129**(4): p. 1756-1771.
878 47. de Brito, O.M. and L. Scorrano, *Mitofusin 2 tethers endoplasmic reticulum to*
879   *mitochondria.* Nature, 2008. **456**(7222): p. 605-10.
880 48. Aumeier, C., et al., *Self-repair promotes microtubule rescue.* Nat Cell Biol, 2016. **18**(10):
881   p. 1054-1064.
882 49. Atherton, J., et al., *Microtubule architecture in vitro and in cells revealed by cryo-electron*
883   *tomography.* Acta Crystallogr D Struct Biol, 2018. **74**(Pt 6): p. 572-584.
884 50. Triclin, S., et al., *Self-repair protects microtubules from destruction by molecular motors.*
885   Nat Mater, 2021. **20**(6): p. 883-891.
886 51. Andreu-Carbo, M., et al., *Motor usage imprints microtubule stability along the shaft.* Dev
887   Cell, 2022. **57**(1): p. 5-18 e8.
888 52. Zilberman, Y., et al., *Regulation of microtubule dynamics by inhibition of the tubulin*
889   *deacetylase HDAC6.* J Cell Sci, 2009. **122**(Pt 19): p. 3531-41.
890 53. Bartolini, F., et al., *An mDia1-INF2 formin activation cascade facilitated by IQGAP1*
891   *regulates stable microtubules in migrating cells.* Mol Biol Cell, 2016. **27**(11): p. 1797-808.
892 54. Area-Gomez, E., et al., *Upregulated function of mitochondria-associated ER membranes*
893   *in Alzheimer disease.* EMBO J, 2012. **31**(21): p. 4106-23.
894 55. Area-Gomez, E. and E.A. Schon, *On the Pathogenesis of Alzheimer's Disease: The MAM*
895   *Hypothesis.* FASEB J, 2017. **31**(3): p. 864-867.
896 56. Montesinos, J., et al., *The Alzheimer's disease-associated C99 fragment of APP regulates*
897   *cellular cholesterol trafficking.* EMBO J, 2020. **39**(20): p. e103791.
898 57. Bienias, K., et al., *Regulation of sphingomyelin metabolism.* Pharmacol Rep, 2016. **68**(3):
899   p. 570-81.
900 58. Grimm, M.O., et al., *Regulation of cholesterol and sphingomyelin metabolism by amyloid-*
901   *beta and presenilin.* Nat Cell Biol, 2005. **7**(11): p. 1118-23.
902 59. Barbullushi, K., et al., *Disease Modeling and Therapeutic Strategies in CMT2A: State of*
903   *the Art.* Mol Neurobiol, 2019. **56**(9): p. 6460-6471.
904 60. El Fissi, N., et al., *Mitofusin gain and loss of function drive pathogenesis in Drosophila*
905   *models of CMT2A neuropathy.* EMBO Rep, 2018. **19**(8).

906 61. Zuchner, S., et al., *Mutations in the mitochondrial GTPase mitofusin 2 cause Charcot-*
907   *Marie-Tooth neuropathy type 2A.* Nat Genet, 2004. **36**(5): p. 449-51.
908 62. Chung, K.W., et al., *Early onset severe and late-onset mild Charcot-Marie-Tooth disease*
909   *with mitofusin 2 (MFN2) mutations.* Brain, 2006. **129**(Pt 8): p. 2103-18.
910 63. Zuchner, S., et al., *Axonal neuropathy with optic atrophy is caused by mutations in*
911   *mitofusin 2.* Ann Neurol, 2006. **59**(2): p. 276-81.
912 64. Detmer, S.A. and D.C. Chan, *Complementation between mouse Mfn1 and Mfn2 protects*
913   *mitochondrial fusion defects caused by CMT2A disease mutations.* Journal of Cell Biology,
914   2007. **176**(4): p. 405-414.
915 65. Devine, M.J., N. Birsa, and J.T. Kittler, *Miro sculpts mitochondrial dynamics in neuronal*
916   *health and disease.* Neurobiol Dis, 2016. **90**: p. 27-34.
917 66. Davis, K., et al., *Miro GTPase domains regulate the assembly of the mitochondrial motor-*
918   *adaptor complex.* Life Sci Alliance, 2023. **6**(1).
919 67. Park, H.J., et al., *A novel INF2 mutation in a Korean family with autosomal dominant*
920   *intermediate Charcot-Marie-Tooth disease and focal segmental glomerulosclerosis.* J
921   Peripher Nerv Syst, 2014. **19**(2): p. 175-9.
922 68. Davenport, A.M., et al., *Structural and functional characterization of the alpha-tubulin*
923   *acetyltransferase MEC-17.* J Mol Biol, 2014. **426**(14): p. 2605-16.
924 69. Pero, M.E., et al., *Pathogenic role of delta 2 tubulin in bortezomib-induced peripheral*
925   *neuropathy.* Proceedings of the National Academy of Sciences of the United States of
926   America, 2021. **118**(4).
927 70. Qu, X., et al., *Activity-Dependent Nucleation of Dynamic Microtubules at Presynaptic*
928   *Boutons Controls Neurotransmission.* Curr Biol, 2019. **29**(24): p. 4231-4240 e5.
929 71. Khawaja, S., G.G. Gundersen, and J.C. Bulinski, *Enhanced stability of microtubules*
930   *enriched in detyrosinated tubulin is not a direct function of detyrosination level.* J Cell
931   Biol, 1988. **106**(1): p. 141-9.
932 72. Bligh, E.G. and W.J. Dyer, *A rapid method of total lipid extraction and purification.* Can
933   J Biochem Physiol, 1959. **37**(8): p. 911-7.
934 73. Vance, J.E., *Phosphatidylserine and phosphatidylethanolamine in mammalian cells: two*
935   *metabolically related aminophospholipids.* J Lipid Res, 2008. **49**(7): p. 1377-87.
936 74. Shin, G.J., et al., *Integrins protect sensory neurons in models of paclitaxel-induced*
937   *peripheral sensory neuropathy.* Proc Natl Acad Sci U S A, 2021. **118**(15).

938